European Congress on Computational Methods
in Applied Sciences and Engineering (ECCOMAS 2012)
J. Eberhardsteiner et.al. (eds.)
Vienna, Austria, September 10-14, 2012

MIXED 3D BEAM MODELS: DIFFERENTIAL EQUATION DERIVATION AND FINITE ELEMENT SOLUTIONS

Ferdinando Auricchio[1,2]**, Giuseppe Balduzzi**[3] **and Carlo Lovadina**[3]

[1] DICAR - Dipartimento di Ingegneria Civile e Architettura, Università degli studi di Pavia
via Ferrata 1, 27100 Pavia PV Italy
e-mail: ferdinando.auricchio@unipv.it,

[2] CeSNA - Centro di Simulazione Numerica Avanzata, Istituto Universitario di Studi Superiori Pavia
viale Lungo Ticino Sforza 56, 27100 Pavia PV Italy,

[3] DIMAT - Dipartimento di Matematica "F. Casorati", Università degli studi di Pavia
via Ferrata 1, 27100 Pavia PV Italy
e-mail: {giuseppe.balduzzi,carlo.lovadina}@unipv.it

Keywords: Hellinger-Reissner principle, 3D beam model, dimensional reduction, mixed beam finite element

Abstract. *In this document we illustrate the dimensional-reduction approach applied to 3D solid elastic equations in order to obtain a beam model.*
We start from the Hellinger-Reissner (HR) principle, in a formulation which guarantees the selection of a compatible solution in a family of equilibrated fields. Then, we introduce a semi-discretization within the cross-section, this allows to reduce the problem's dimension from 3D to 1D and to formulate the properly called beam model. After a manipulation of the 1D weak model (done in order to guarantee the selection of an axis-equilibrated solution in a family of axis-compatible fields), we introduce a discretization also along the beam axis obtaining the related beam Finite Element (FE).

On one hand, the initial HR principle formulation leads to an accurate stress analysis into the cross-section, on the other hand, the 1D model manipulation leads to an accurate displacement analysis along the beam-axis. Moreover, the manipulation allows to statically condensate stresses at element level, improving the numerical efficiency of the FE algorithm.

In order to illustrate the capability of the method, we consider a slim cross-section beam that shows interesting non trivial behaviour in bending and for which the analytical solution is available in literature. Numerical results are accurate in description of both displacement and stress variables, the FE solution converges to the analytical solution, and the beam FE models complex phenomena like anticlastic bending and boundary effects.

1 INTRODUCTION

In Reference [2] the authors develop a planar beam-model and the correspondent beam Finite Element (FE) applying a procedure structured in four main steps, listed in the following. The main aim of the procedure is to obtain a simple beam model and the corresponding FE capable of capturing the cross-section stress distribution with high accuracy.

(a) **Formulation of the 2D linear elastic problem.** The authors propose the Hellinger-Reissner (HR) principle, a mixed formulation which considers displacement and stress as independent variables. In particular, the authors introduce two possible HR principle formulations: the first uses the gradient of displacements while the latter uses the divergence of stresses. The divergence formulation seems to be the most interesting respect to the procedure goals, since it requires equilibrium on stresses as essential condition and weakly imposes compatibility on displacements.

(b) **Dimensional reduction.** The authors introduce an approximation and integrate within the cross-section, obtaining a properly called 1D *beam model*.

(c) **Manipulation of the beam-model weak formulation.** Integrating by parts, the authors apply axial derivative to displacements. As a consequence displacement axial compatibility becomes essential condition and axial equilibrium on stresses is weakly enforced.

(d) **FE discretization.** The authors introduce an axial approximation and integrate along the beam axis, obtaining the beam FE.

The *dimensional reduction* is a mathematical, general procedure formulated firstly in Reference [6] and usable in many applicative fields. In particular, in References [9] and [10], the authors apply the dimensional reduction to 3D elastic solid equations in order to obtain a plate model. They provide an a posteriori model error estimation and use it to choose optimal basis functions. More recently, other researchers use the dimensional reduction in their beam- and plate- model derivation, considering also a more complicated initial problem (e.g., see References [3], [4]).
We remark that the dimensional reduction allows to avoid restrictive hypothesis in the beam-model derivation. As a consequence, the model accuracy could be improved arbitrarily and the procedure should be easily generalized to more complex situations such as non-linear constitutive laws or thermal coupled problems.

Trough Step (c), the procedure introduced at the beginning of this section gives the opportunity to manipulate the weak formulation in order to optimize the structure of spaces where the solution lives. As a consequence, the authors can exploit the initial HR formulation in order to achieve the work's aims, but obtain a displacement-based FE formulation, as explained in Reference [2] and also in the following.

In Reference [2], the authors highlight others advantages of the procedure, such as the accuracy of stress description in numerical results, the convergence of numerical results to the analytical solution, and the capability of the method to catch the boundary effects. It is worth noting that correction factors are not required in the obtained beam models.

In this document we generalize the so far introduced procedure to the 3D case. To this aim, we consider only elastic homogeneous body and simple cross-section geometries whereas more complicated models will be investigated in further studies.

2 PROBLEM FORMULATION

We investigate a 3D linear elastic, homogeneous, and isotropic body Ω subjected to small displacements. More in detail, we consider only prismatic bodies which we refer to as *beams*. Specifically, the beam is defined as:

$$\Omega := l \times A \tag{1}$$

with $l \subset \mathbb{R}$ the beam longitudinal axis and $A \subset \mathbb{R}^2$ the beam cross-section that we assume to be orthogonal, closed, and bounded sets. Figure 1 represents the domain, the reference Cartesian coordinate system, the left-hand side and the right-hand side cross-sections A_0 and A_l, and the lateral surface $L := \partial A \times l$ where ∂A is the cross-section boundary.

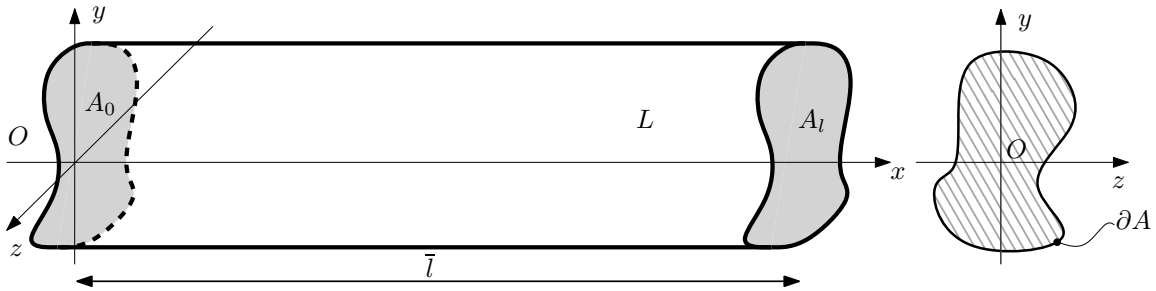

Figure 1: 3D beam geometry, coordinate system, dimensions, and adopted notations.

Denoting the domain boundary as $\partial\Omega$, we consider its partition $\{\partial\Omega_t; \partial\Omega_s\}$ with $\partial\Omega_t := L \cup A_l$ the externally loaded boundary and $\partial\Omega_s := A_0$ the displacement constrained boundary.

We impose to the beam the body and the external loads, $\boldsymbol{f} : \Omega \to \mathbb{R}^3$ and $\boldsymbol{t} : \partial\Omega_t \to \mathbb{R}^3$ respectively, as well as a sufficiently smooth boundary displacement function $\overline{\boldsymbol{s}} : \partial\Omega_s \to \mathbb{R}^3$. Introducing the symmetric stress tensor field $\boldsymbol{\sigma} : \Omega \to \mathbb{R}^{3\times3}_s$ and the displacement vector field $\boldsymbol{s} : \Omega \to \mathbb{R}^3$, the investigated problem can be formulated as follows

$$\begin{aligned} &\text{Find } \boldsymbol{s} \in W \text{ and } \boldsymbol{\sigma} \in S_t \text{ such that } \forall\, \delta\boldsymbol{s} \in W \text{and } \forall\, \delta\boldsymbol{\sigma} \in S_0 \\ &\delta J_{HR} := -\int_\Omega \delta\boldsymbol{s} \cdot \nabla \cdot \boldsymbol{\sigma}\, d\Omega - \int_\Omega \nabla \cdot \delta\boldsymbol{\sigma} \cdot \boldsymbol{s}\, d\Omega - \int_\Omega \delta\boldsymbol{\sigma} : \boldsymbol{D}^{-1} : \boldsymbol{\sigma}\, d\Omega \\ &\qquad\qquad - \int_\Omega \delta\boldsymbol{s} \cdot \boldsymbol{f}\, d\Omega + \int_{\partial\Omega_s} \delta\boldsymbol{\sigma} \cdot \boldsymbol{n} \cdot \overline{\boldsymbol{s}}\, dS = 0 \end{aligned} \tag{2}$$

with $\boldsymbol{D}$ the fourth order linear elastic tensor and

$$\begin{aligned} &W := \left\{\boldsymbol{s} \in L^2(\Omega)\right\} \\ &S_t := \left\{\boldsymbol{\sigma} \in H(\mathrm{div}, \Omega) : \boldsymbol{\sigma} \cdot \boldsymbol{n}|_{\partial\Omega_t} = \boldsymbol{t}\right\}; \quad S_0 := \left\{\delta\boldsymbol{\sigma} \in H(\mathrm{div}, \Omega) : \delta\boldsymbol{\sigma} \cdot \boldsymbol{n}|_{\partial\Omega_t} = \boldsymbol{0}\right\} \end{aligned} \tag{3}$$

We highlight that, since $\boldsymbol{\sigma} \in H(\mathrm{div}, \Omega)$ and $\boldsymbol{s} \in L^2(\Omega)$, the HR functional stationarity (2) privileges the regularity of stress components, in accordance with the study aims. Unfortunately, space definitions imply that, in an hypothetical FE discretization, displacements could be discontinuous whereas stress components should have some inter-element continuity. As a consequence the assembling procedure must be done considering stress variables and the FE discretization results non compatible with the usual displacement-based FE.

The HR functional stationarity (2) is deeply investigated in the mathematical literature: a classical Reference is [5] in which the authors provide necessary conditions to ensure that Problem (2) is *well-posed*. Moreover, with respect to the FE approximation, the authors give an error

estimation and prove the convergence of both variables $\boldsymbol{s}$ and $\boldsymbol{\sigma}$.
Despite its advantages, the applications of the HR functional stationarity (2) to engineering problems are not so diffused. The motivations could be: (i) the non-trivial conditions on the dimension and regularity of both spaces W and S to ensure that the problem is well-posed, (ii) the complexity of the FE shape functions approximating the $H(\mathrm{div}, \Omega)$ space that may be cumbersome for numerical manipulation.

3 DIMENSIONAL REDUCTION

In this section we introduce some cross-section approximated fields in the HR functional stationarity (2) and we perform a cross-section integration in order to reduce the problem dimension (i.e. to develop the properly called beam model).

3.1 Cross-section approximations and notations

To approximate a generic scalar field $\gamma(x, y, z)$ involved in the HR functional stationarity (2), we express it as a linear combination of several assigned *cross-section shape functions* $\boldsymbol{r}_\gamma : A \to \mathbb{R}^d$ with undetermined *axial coefficient functions* $\hat{\boldsymbol{\gamma}} : l \to \mathbb{R}^d$

$$\gamma(x, y, z) \approx \boldsymbol{r}_\gamma^T \hat{\boldsymbol{\gamma}} \tag{4}$$

with d the number of cross-section shape functions used in the approximation and $(\,\cdot\,)^T$ the transposition operation.

The cross-section shape functions $\boldsymbol{r}_\gamma$ are a set of linearly independent functions; as a consequence, the field $\gamma(x, y, z)$ is uniquely determined by the components of $\hat{\boldsymbol{\gamma}}$ that are indeed the *unknowns* of the developed beam model. Adopting Position (4) and using the engineering notation, displacement and stress fields are given, respectively, by

$$\boldsymbol{s} := \begin{Bmatrix} s_u \\ s_v \\ s_w \end{Bmatrix} \approx \begin{bmatrix} \boldsymbol{r}_u^T & \boldsymbol{0} & \boldsymbol{0} \\ \boldsymbol{0} & \boldsymbol{r}_v^T & \boldsymbol{0} \\ \boldsymbol{0} & \boldsymbol{0} & \boldsymbol{r}_w^T \end{bmatrix} \begin{Bmatrix} \hat{\boldsymbol{u}} \\ \hat{\boldsymbol{v}} \\ \hat{\boldsymbol{w}} \end{Bmatrix} = \boldsymbol{R}_s \hat{\boldsymbol{s}} \tag{5}$$

$$\boldsymbol{\sigma} := \begin{Bmatrix} \sigma_{xx} \\ \sigma_{yy} \\ \sigma_{zz} \\ \tau_{xy} \\ \tau_{xz} \\ \tau_{yz} \end{Bmatrix} \approx \begin{bmatrix} \boldsymbol{r}_{\sigma_x}^T & \boldsymbol{0} & \boldsymbol{0} & \boldsymbol{0} & \boldsymbol{0} & \boldsymbol{0} \\ \boldsymbol{0} & \boldsymbol{r}_{\sigma_y}^T & \boldsymbol{0} & \boldsymbol{0} & \boldsymbol{0} & \boldsymbol{0} \\ \boldsymbol{0} & \boldsymbol{0} & \boldsymbol{r}_{\sigma_z}^T & \boldsymbol{0} & \boldsymbol{0} & \boldsymbol{0} \\ \boldsymbol{0} & \boldsymbol{0} & \boldsymbol{0} & \boldsymbol{r}_{\tau_{xy}}^T & \boldsymbol{0} & \boldsymbol{0} \\ \boldsymbol{0} & \boldsymbol{0} & \boldsymbol{0} & \boldsymbol{0} & \boldsymbol{r}_{\tau_{xz}}^T & \boldsymbol{0} \\ \boldsymbol{0} & \boldsymbol{0} & \boldsymbol{0} & \boldsymbol{0} & \boldsymbol{0} & \boldsymbol{r}_{\tau_{yz}}^T \end{bmatrix} \begin{Bmatrix} \hat{\boldsymbol{\sigma}}_x \\ \hat{\boldsymbol{\sigma}}_y \\ \hat{\boldsymbol{\sigma}}_z \\ \hat{\boldsymbol{\tau}}_{xy} \\ \hat{\boldsymbol{\tau}}_{xz} \\ \hat{\boldsymbol{\tau}}_{yz} \end{Bmatrix} = \boldsymbol{R}_\sigma \hat{\boldsymbol{\sigma}} \tag{6}$$

In the same way, virtual displacement and stress fields become:

$$\delta\boldsymbol{s} = \boldsymbol{R}_s \delta\hat{\boldsymbol{s}}; \quad \delta\boldsymbol{\sigma} = \boldsymbol{R}_\sigma \delta\hat{\boldsymbol{\sigma}} \tag{7}$$

In agreement with the engineering notation, we re-define the differential operator and the normal unit vector product:

Tensor notation		Engineering notation	
$\nabla \cdot \boldsymbol{\sigma}$	$\equiv$	$\dfrac{\partial}{\partial x}\boldsymbol{E}_1 \boldsymbol{R}_\sigma \hat{\boldsymbol{\sigma}} + \dfrac{\partial}{\partial y}\boldsymbol{E}_2 \boldsymbol{R}_\sigma \hat{\boldsymbol{\sigma}} + \dfrac{\partial}{\partial z}\boldsymbol{E}_3 \boldsymbol{R}_\sigma \hat{\boldsymbol{\sigma}}$	(8)
$\boldsymbol{\sigma} \cdot \boldsymbol{n}$	$\equiv$	$(n_x \boldsymbol{E}_1 + n_y \boldsymbol{E}_2 + n_z \boldsymbol{E}_3)\, \boldsymbol{R}_\sigma \hat{\boldsymbol{\sigma}}$	(9)

where

$$\boldsymbol{E}_1 = \begin{bmatrix} 1 & 0 & 0 & 0 & 0 & 0 \\ 0 & 0 & 0 & 1 & 0 & 0 \\ 0 & 0 & 0 & 0 & 1 & 0 \end{bmatrix}; \quad \boldsymbol{E}_2 = \begin{bmatrix} 0 & 0 & 0 & 1 & 0 & 0 \\ 0 & 1 & 0 & 0 & 0 & 0 \\ 0 & 0 & 0 & 0 & 0 & 1 \end{bmatrix}; \quad \boldsymbol{E}_3 = \begin{bmatrix} 0 & 0 & 0 & 0 & 1 & 0 \\ 0 & 0 & 0 & 0 & 0 & 1 \\ 0 & 0 & 1 & 0 & 0 & 0 \end{bmatrix} \tag{10}$$

In the matrix form, the fourth order linear elastic tensor $\boldsymbol{D}^{-1}$ is defined as follows:

$$\boldsymbol{D}^{-1} := \frac{1}{E} \begin{bmatrix} 1 & -\nu & -\nu & 0 & 0 & 0 \\ -\nu & 1 & -\nu & 0 & 0 & 0 \\ -\nu & -\nu & 1 & 0 & 0 & 0 \\ 0 & 0 & 0 & 2(1+\nu) & 0 & 0 \\ 0 & 0 & 0 & 0 & 2(1+\nu) & 0 \\ 0 & 0 & 0 & 0 & 0 & 2(1+\nu) \end{bmatrix} \tag{11}$$

with E the Young's modulus and ν the Poisson's ratio which define the linear elastic properties of the material constituting the body.
Due to assumption (4), computation of partial derivatives is straightforward:

$$\frac{\partial}{\partial x}\gamma = \boldsymbol{r}_\gamma^T \frac{d}{dx}\hat{\boldsymbol{\gamma}} = \boldsymbol{r}_\gamma^T \hat{\boldsymbol{\gamma}}'; \quad \frac{\partial}{\partial y}\gamma = \frac{\partial}{\partial y}\boldsymbol{r}_\gamma^T \hat{\boldsymbol{\gamma}} = \boldsymbol{r}_{\gamma,y}^T \hat{\boldsymbol{\gamma}}; \quad \frac{\partial}{\partial z}\gamma = \frac{\partial}{\partial z}\boldsymbol{r}_\gamma^T \hat{\boldsymbol{\gamma}} = \boldsymbol{r}_{\gamma,z}^T \hat{\boldsymbol{\gamma}} \tag{12}$$

where the prime means the derivative along x whereas $(\cdot)_{,y}$ and $(\cdot)_{,z}$ mean the derivatives along y and z respectively.

3.2 Model formulation

We assume that the lateral surface L is unloaded, i.e. $\boldsymbol{t}|_L = \boldsymbol{0}$. Moreover, since we need to satisfy exactly the boundary equilibrium (see S_t definition (3)), we assume also that $\boldsymbol{t}|_{A_l}$ can be represented using the assigned profiles $\boldsymbol{R}_\sigma$. This means that there exist suitable vectors $\hat{\boldsymbol{t}}_x$, $\hat{\boldsymbol{t}}_y$, and $\hat{\boldsymbol{t}}_z$ such that

$$\boldsymbol{t}|_{A_l} = \left\{ \begin{array}{c} \boldsymbol{r}_{\sigma_x}^T \hat{\boldsymbol{t}}_x \\ \boldsymbol{r}_{\tau_{xy}}^T \hat{\boldsymbol{t}}_y \\ \boldsymbol{r}_{\tau_{xz}}^T \hat{\boldsymbol{t}}_z \end{array} \right\} \tag{13}$$

At this point, we perform some substitutions, manipulations, and integrations. In particular we introduce the engineering notations (8) and (9) and the approximations (5) and (6) into HR functional stationarity (2), we develop algebraic products and we split integrals on the domain Ω into integrals along the axis l and integrals on the cross section A. Consequently, HR functional stationarity (2) could be expressed as

$$\begin{aligned} \delta J_{HR} = -\int_l \left(\delta\hat{\boldsymbol{s}}^T \boldsymbol{G}_{s\sigma}\hat{\boldsymbol{\sigma}}' + \delta\hat{\boldsymbol{s}}^T \boldsymbol{H}_{s\sigma}\hat{\boldsymbol{\sigma}} + \delta\hat{\boldsymbol{\sigma}}'^T \boldsymbol{G}_{\sigma s}\hat{\boldsymbol{s}} + \delta\hat{\boldsymbol{\sigma}}^T \boldsymbol{H}_{\sigma s}\hat{\boldsymbol{s}} + \delta\hat{\boldsymbol{\sigma}}^T \boldsymbol{H}_{\sigma\sigma}\hat{\boldsymbol{\sigma}} + \delta\hat{\boldsymbol{s}}^T \boldsymbol{F} \right) dx \\ -\delta\hat{\boldsymbol{\sigma}}^T \overline{\boldsymbol{S}} = 0 \end{aligned} \tag{14}$$

where we defined

$$\begin{aligned} &\boldsymbol{H}_{s\sigma} = \boldsymbol{H}_{\sigma s}^T = \int_A \left(\boldsymbol{R}_s^T \boldsymbol{E}_2 \boldsymbol{R}_{\sigma,y} + \boldsymbol{R}_s^T \boldsymbol{E}_3 \boldsymbol{R}_{\sigma,z} \right) dS; \quad \boldsymbol{H}_{\sigma\sigma} = \int_A \boldsymbol{R}_\sigma^T \boldsymbol{D}^{-1} \boldsymbol{R}_\sigma dS \\ &\boldsymbol{G}_{s\sigma} = \boldsymbol{G}_{\sigma s}^T = \int_A \boldsymbol{R}_s^T \boldsymbol{E}_1 \boldsymbol{R}_\sigma dS; \quad \boldsymbol{F} = \int_A \boldsymbol{R}_s^T \boldsymbol{f} dS; \quad \overline{\boldsymbol{S}} = \int_{A_0} \boldsymbol{R}_\sigma^T \boldsymbol{E}_1 \overline{\boldsymbol{s}} dS \end{aligned} \tag{15}$$

Since cross-section shape functions $\boldsymbol{r}_\gamma$ are assigned, matrices $\boldsymbol{H}_{s\sigma}$, $\boldsymbol{H}_{\sigma\sigma}$, and $\boldsymbol{G}_{s\sigma}$ become constant-coefficient matrices, playing the role of the beam stiffness.
Equation (14) represents the so called *1D beam model weak formulation*.

4 FE DERIVATION

In order to obtain the beam FE formulation we start from the beam model variational formulation (14). Assuming $\overline{\boldsymbol{s}} = \boldsymbol{0}$ and integrating by parts with respect to the x direction both the first and the third terms, we obtain the following, alternative beam model formulation:

$$\begin{aligned}&\text{Find } \hat{\boldsymbol{s}} \in \widetilde{W} \text{ and } \hat{\boldsymbol{\sigma}} \in \widetilde{S} \text{ such that } \forall\, \delta\hat{\boldsymbol{s}} \in \widetilde{W} \text{ and } \forall\, \delta\hat{\boldsymbol{\sigma}} \in \widetilde{S}\\ &\delta J_{HR} = \int_l \left(\delta\hat{\boldsymbol{s}}'^T \boldsymbol{G}_{s\sigma}\hat{\boldsymbol{\sigma}} - \delta\hat{\boldsymbol{s}}^T \boldsymbol{H}_{s\sigma}\hat{\boldsymbol{\sigma}} + \delta\hat{\boldsymbol{\sigma}}^T \boldsymbol{G}_{\sigma s}\hat{\boldsymbol{s}}' - \delta\hat{\boldsymbol{\sigma}}^T \boldsymbol{H}_{\sigma s}\hat{\boldsymbol{s}} - \delta\hat{\boldsymbol{\sigma}}^T \boldsymbol{H}_{\sigma\sigma}\hat{\boldsymbol{\sigma}} - \delta\hat{\boldsymbol{s}}^T \boldsymbol{F}\right) dx \\ &\qquad\qquad - \delta\hat{\boldsymbol{s}}^T \boldsymbol{T} = 0\end{aligned} \tag{16}$$

with $\widetilde{W} := \{\hat{\boldsymbol{s}} \in H^1(l) : \hat{\boldsymbol{s}}|_{x=0} = \boldsymbol{0}\}$; $\widetilde{S} := L^2(l)$ and $\boldsymbol{T} = \int_{A_l} \boldsymbol{R}_s^T \boldsymbol{t} dA$

It is interesting to highlight the following statements.

- $x-$ derivatives applied to displacement variables together with the definition of $\widetilde{W}$ – in which the axial compatibility is the *essential* condition – lead to a formulation that guarantees the selection of an axis equilibrated solution in a family of axis compatible fields.
- $y-$ and $z-$ derivatives applied to stress variables (see $\boldsymbol{H}_{s\sigma}$ definition (15)) together with the definition of S_t – in which cross-section equilibrium is the *essential* condition – lead to a formulation that guarantees the selection of a cross-section compatible solution in a family of cross-section equilibrate fields.
- The weak formulation is symmetric.

In order to construct the FE approximation of the i-th axial coefficient function $\hat{\gamma}_i$, involved in the beam model weak formulation (16), we express it as a linear combination of some assigned *axis shape functions* $\boldsymbol{N}_{\gamma i} : l \to \mathbb{R}^t$ with unknown *numerical coefficients* $\widetilde{\boldsymbol{\gamma}}_i \in \mathbb{R}^t$:

$$\hat{\boldsymbol{\gamma}}(x) \approx \boldsymbol{N}_\gamma \widetilde{\boldsymbol{\gamma}} \tag{17}$$

where

$$\boldsymbol{N}_\gamma = \begin{bmatrix} \boldsymbol{N}_{\gamma 1}^T & \boldsymbol{0} & \cdots & \boldsymbol{0} \\ \boldsymbol{0} & \boldsymbol{N}_{\gamma 2}^T & \cdots & \boldsymbol{0} \\ \vdots & \vdots & \ddots & \vdots \\ \boldsymbol{0} & \boldsymbol{0} & \cdots & \boldsymbol{N}_{\gamma d}^T \end{bmatrix}; \quad \widetilde{\boldsymbol{\gamma}} = \begin{Bmatrix} \widetilde{\boldsymbol{\gamma}}_1 \\ \widetilde{\boldsymbol{\gamma}}_2 \\ \vdots \\ \widetilde{\boldsymbol{\gamma}}_d \end{Bmatrix} \tag{18}$$

The FE discretization of the model follows from the introduction of the axis shape function approximation (17) into the variational formulation (16). Collecting unknown coefficients in a vector and requiring the satisfaction of Equation (16) for all possible virtual fields, we obtain the following algebraic system:

$$\begin{bmatrix} \boldsymbol{0} & \boldsymbol{K}_{s\sigma} \\ \boldsymbol{K}_{\sigma s} & \boldsymbol{K}_{\sigma\sigma} \end{bmatrix} \begin{Bmatrix} \widetilde{\boldsymbol{s}} \\ \widetilde{\boldsymbol{\sigma}} \end{Bmatrix} = \begin{Bmatrix} \widetilde{\boldsymbol{T}} \\ \boldsymbol{0} \end{Bmatrix} \tag{19}$$

where

$$\boldsymbol{K}_{s\sigma} = \boldsymbol{K}_{\sigma s}^T = \int_l \left(\boldsymbol{N}_s'^T \boldsymbol{G}_{s\sigma} \boldsymbol{N}_\sigma - \boldsymbol{N}_s^T \boldsymbol{H}_{s\sigma} \boldsymbol{N}_\sigma \right) dx \tag{20}$$

$$\boldsymbol{K}_{\sigma\sigma} = -\int_l \boldsymbol{N}_\sigma^T \boldsymbol{H}_{\sigma\sigma} \boldsymbol{N}_\sigma dx; \quad \widetilde{\boldsymbol{T}} = -\int_l \boldsymbol{N}_s^T \boldsymbol{F} dx - \boldsymbol{N}_s^T \big|_{x=\bar{l}} \boldsymbol{T} \tag{21}$$

5 SHAPE FUNCTION DEFINITIONS

In Reference [1], in order to ensure that the beam model is *well-posed*, the authors indicate as a possible choice the following condition:

$$\nabla \cdot S_0 = W \tag{22}$$

Unfortunately, to define cross-section shape functions over a generic cross-section geometry which approximate S_0 and satisfy condition (22) is not trivial. Consequently, we limit our attention to simple cross-section geometries, specifically we require that the cross-section could be divided in elementary rectangles, as illustrated in Figure 2.

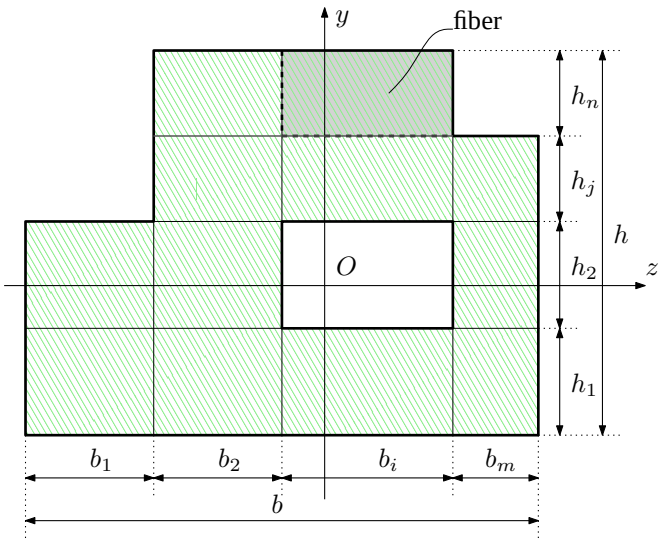

Figure 2: Cross-section geometry definition, coordinate system, dimensions, and adopted notations.

The simplest case we can consider is a prismatic beam with a rectangular cross-section:

$$A = \left\{ (y; z) \in \mathbb{R}^2 \quad | \quad y \in \left[-\frac{h}{2}, \frac{h}{2} \right] \text{ and } \quad z \in \left[-\frac{b}{2}, \frac{b}{2} \right] \right\} \tag{23}$$

with h the thickness and b is the depth of the beam.
In this case, the cross-section shape functions may be defined as the tensor product of two *profile function vectors* $\boldsymbol{p}_\gamma(y)$ and $\boldsymbol{q}_\gamma(z)$:

$$\boldsymbol{p}_\gamma : h \to \mathbb{R}^g; \quad \boldsymbol{q}_\gamma : b \to \mathbb{R}^k; \quad \boldsymbol{r}_\gamma := \text{vec}\left(\boldsymbol{p}_\gamma(y) \, \boldsymbol{q}_\gamma^T(z) \right) \tag{24}$$

where $\text{vec}(\cdot)$ is the linear operator that reshapes a tensor into a column vector.

We assume that the profile functions are complete polynomials and we denote with $\deg(\cdot)$ their maximum degree. Introducing the profile function definition (24) into the condition (22), we obtain the profile vector properties summarized in Table 1.

We can build non-elementary cross-sections assembling elementary rectangular blocks (called *fibres*). The fibre assembling can be implemented imposing to each profile function the continuity specified in Table 1.

In order to ensure that the beam FE is well-posed and stable, according to the condition (22), we choice $\widetilde{W}$ and $\widetilde{S}$ such that

$$\frac{d}{dx}\widetilde{W} = \widetilde{S} \tag{25}$$

Being also axis shape functions complete polynomials and introducing the axis shape function definition (17) into the condition (25), we obtain the axis shape-function properties summarized in Table 1, together with properties of profile vectors. During the FE assembling procedure we must impose axial continuity on displacements, as specified in Table 1.

Variable	$\deg(\boldsymbol{p}_\gamma)$	y continuity	$\deg(\boldsymbol{q}_\gamma)$	z continuity	$\deg(\boldsymbol{N}_\gamma)$	x continuity
u	1	C^{-1}	1	C^{-1}	2	C^0
v	2	C^{-1}	1	C^{-1}	3	C^0
w	1	C^{-1}	2	C^{-1}	3	C^0
σ_x	1	C^{-1}	1	C^{-1}	1	C^{-1}
σ_y	3	C^0	1	C^{-1}	3	C^{-1}
σ_z	1	C^{-1}	3	C^0	3	C^{-1}
τ_{xy}	2	C^0	1	C^{-1}	2	C^{-1}
τ_{xz}	1	C^{-1}	2	C^0	2	C^{-1}
τ_{yz}	2	C^0	2	C^0	3	C^{-1}

Table 1: Degree and continuity of cross-section profile vectors and axis shape functions (C^{-1} means discontinuous function).

It is worth noting that, since all stress components are discontinuous along the beam-axis, it is possible to statically condensate them out at element level, reducing significantly the dimension of global stiffness matrix and improving the FE algorithm efficiency.

6 NUMERICAL RESULTS

To illustrate the model capability we consider the bending of a beam with the slim cross-section represented in Figure 3. We choose this example since the beam shows interesting non trivial behaviours in bending and its analytical solution is available in literature.

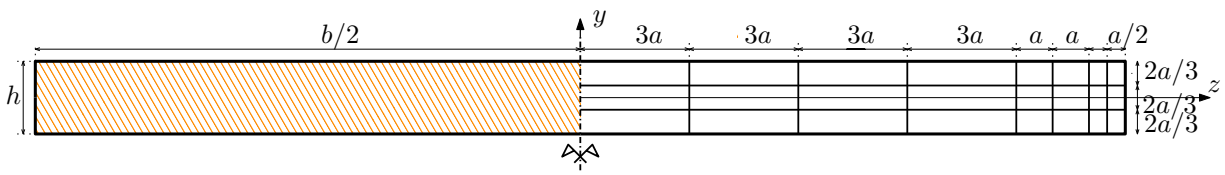

Figure 3: Slim cross section: geometry and mesh definition.

The beam geometrical dimensions are $h = 0.2\text{mm}$, $b = 3\text{mm}$, and $\bar{l} = 20\text{mm}$ whereas $a = 0.1\text{mm}$. The beam is clamped in the left-hand side cross section A_0 (i.e., $\overline{\boldsymbol{s}} = \boldsymbol{0}$, as already specified in Section 4) and loaded in the right-hand side cross section A_l by a distributed shear load (i.e., $\boldsymbol{f} = \boldsymbol{0}$ and $\boldsymbol{t} = \{0, -1, 0\}^T\,\text{MPa}$). The material parameters are: $E = 10^5\,\text{MPa}$ and $\nu = 0.25$. Finally, the axis discretization is done through a regular mesh of 10 elements whereas

the cross-section discretization is done through 48 non regular rectangular fibres with more fine grid where complex phenomena occur. However, this aspect will be more clear at the end of this section.

Figure 4 plots the deformed cross-section at $x = 10\text{mm}$ (to highlight deformations, displacements are amplified of a factor 10).
It is interesting to notice the following statements.

- Discontinuities between fibres in transversal displacement fields s_v and s_w are evident. They are the consequence of the assumption of Table 1 (we let the displacement cross-section shape functions violate the compatibility into the cross section).
- The deformed section is concave, whereas the deformed beam axis is convex. This phenomenon is known in literature as *anticlastic bending* and it becomes more and more significant for higher values of the ratio b/h. It is worth noting that this phenomena is usually ignored in structural design and analysis because the adopted beam models are not able to catch it. Nevertheless, in practical applications, it can be of interest for the induced deformations (see Reference [7]) but also for the induced stress. We clarify this aspect in the following.

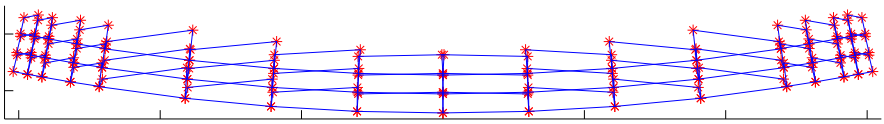

Figure 4: Transversal cross-section displacements (amplification factor 10) evaluated at $x = 10\text{mm}$

Figures 5(a) and 5(c) plot the cross-section shear distributions $\tau_{xy}(10, y, z)$ and $\tau_{xz}(10, y, z)$ respectively.

Since the cross-section, as well as the boundary load and the displacement constrain are symmetric respect to both the $y-$ and $z-$ axis, it is not surprising to obtain symmetric stress distributions. In particular τ_{xy} has an even distribution respect to both the cross-section axis, i.e. $\tau_{xy}(10, y, z) = \tau_{xy}(10, -y, z) = \tau_{xy}(10, y, -z)$, whereas τ_{xz} has an odd distribution respect to both the cross-section axis, i.e. $\tau_{xz}(10, y, z) = -\tau_{xz}(10, -y, z) = -\tau_{xz}(10, y, -z)$. For this reason, in Figures 5, we plot distributions only for $y, z > 0$ in a dimensionless coordinate system.

Due to the cross-section's geometry with high ratio b/h, the shear component τ_{xz} becomes of the same order of magnitude of the other component τ_{xy}. As evidenced in Reference [8], if the analytical solution is considered, the ratio $\max_{(y,z)\in A}(|\tau_{xy}|) \,/\, \max_{(y,z)\in A}(|\tau_{xz}|)$ is close to 1 for the considered b/h ratio. From numerical results the ratio between the maximum shear components results to be equal to 1.03, in agreement with the analytical solution.

The associated relative errors e^{rel}_{xy} and e^{rel}_{xz} are defined both in Equation (26).

$$e^{rel}_{xy} = \frac{\left|\tau_{xy}(10, y, z) - \tau^{ref}_{xy}(10, y, z)\right|}{\max_{(y,z)\in A}\left(\left|\tau^{ref}_{xy}(10, y, z)\right|\right)}; \quad e^{rel}_{xz} = \frac{\left|\tau_{xz}(10, y, z) - \tau^{ref}_{xz}(10, y, z)\right|}{\max_{(y,z)\in A}\left(\left|\tau^{ref}_{xz}(10, y, z)\right|\right)} \tag{26}$$

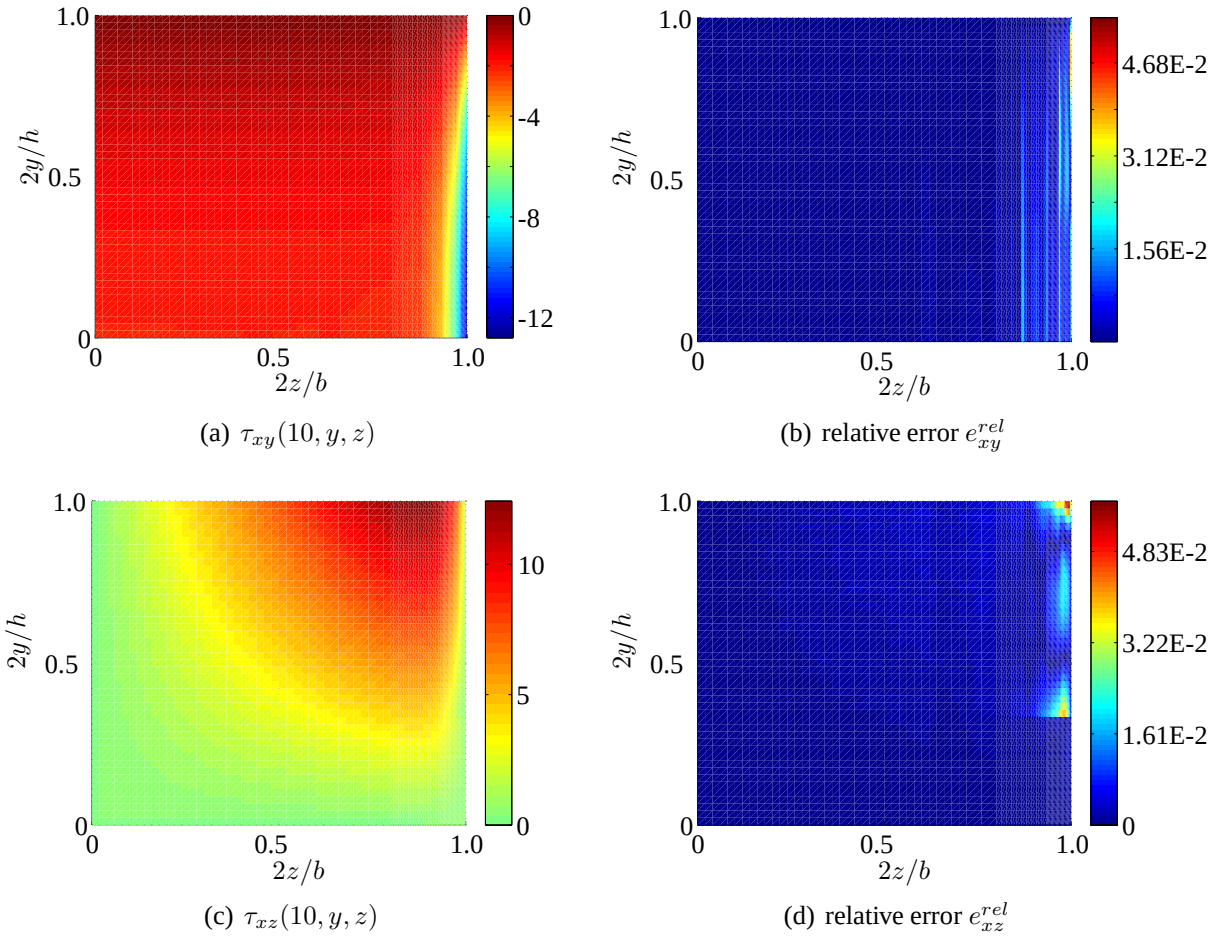

(a) $\tau_{xy}(10, y, z)$ (b) relative error e_{xy}^{rel}

(c) $\tau_{xz}(10, y, z)$ (d) relative error e_{xz}^{rel}

Figure 5: Shear components evaluated at $x = 10\text{mm}$ for the case of homogeneous, slim cross-section: cross-section distributions 5(a) and 5(c), cross-section relative error distributions 5(b) and 5(d) (results plotted for $y, z > 0$).

The reference distributions $\tau_{xy}^{ref}(10, y, z)$ and $\tau_{xz}^{ref}(10, y, z)$ are the analytical solutions of the 3D elastic problem provided trough the Saint-Venant beam solution, as well illustrated in Reference [8][Chap. 12]. Specifically, shear distributions $\tau_{xy}^{ref}(10, y, z)$ and $\tau_{xz}^{ref}(10, y, z)$ are expressed as Fourier series that we truncate at a negligible term respect to the machine precision.

Looking at the relative error distributions (Figures 5(b) and 5(d)), we notice how the error is always less than the 5%, and how the higher relative errors are confined close to the edges. On the contrary, the magnitude of the relative error is lower than the 1% on the rest of the cross-section. According our results, we can argue that the numerical solution is reasonably accurate, despite the relatively coarse cross-section mesh.

7 CONCLUSIONS

In this paper we present a 3D beam model and its correspondent FE: starting from the weak problem formulation of the elastic problem (the HR functional stationarity), we obtain the beam model through the dimensional reduction approach. Introducing the axis FE discretization we obtain the numerical scheme used to obtain the results presented in Section 6.
Numerical results highlight the capability of the adopted numerical scheme to describe accurately both displacement and stress fields, giving interesting perspective for further studies. In particular, in authors opinion, the capability of the beam FE to catch accurately shear stress dis-

tributions is promising (despite the quite large computational effort) and it could be extremely useful in further applications of the beam model such as laminated beam analysis and shear stress analysis of non trivial cross-section geometries.

REFERENCES

[1] Stephen M. Alessandrini, Douglas N. Arnold, Richard S. Falk, and Alexandre L. Madureira. Derivation and justification of plate models by variational methods. *CRM Proceedings and Lecture Notes*, 21:1–20, 1999.

[2] Ferdinando Auricchio, Giuseppe Balduzzi, and Carlo Lovadina. A new modelling approach for planar beams: Finite-element solutions based on mixed variational derivations. *Journal of Mechanic of Materials and Structures*, 5:771–794, 2010.

[3] R. C. Batra and S. Vidoli. Higher-order piezoelectric plate theory derived from a three-dimensional variational principle. *AIAA (American Institute of Aeronautics and Astronautics) journal*, 40:91–104, 2002.

[4] R.C. Batra, S. Vidoli, and F. Vestroni. Plane wave solutions and modal analysis in higher order shear and normal deformable plate theories. *Journal of Sound and Vibration*, 257:63–88, 2002.

[5] Franco Brezzi and Michel Fortin. *Mixed and hybrid finite element methods*. Springer-Verlag New York, Inc., New York, NY, USA, 1991.

[6] L.V. Kantorovich and V.I. Krylov. *Approximate methods of higher analysis*. P. Noordhoff LTD, third edition, 1958.

[7] V.I. Kushnir, J.P. Quintana, and P. Georgopoulos. On the sagittal focusing of synchrotron radiation with a double crystal monochromator. *Nuclear Instruments and Methods in Physics Research, section A*, 328:588–591, 1993.

[8] S. Timoshenko and J. N. Goodier. *Theory of Elasticity*. McGraw-Hill, second edition, 1951.

[9] M. Vogelius and I. Babuska. On a dimensional reduction method I. The optimal selection of basis functions. *Mathematics of Computation*, 37:31–46, 1981.

[10] M. Vogelius and I. Babuska. On a dimensional reduction method II. Some approximation-theoretic results. *Mathematics of Computation*, 37:47–68, 1981.